Earth Surf. Dynam. Discuss., 3, 1255–1288, 2015
www.earth-surf-dynam-discuss.net/3/1255/2015/
doi:10.5194/esurfd-3-1255-2015

Earth Surface Dynamics Discussions
Open Access

3-D models and structural analysis of analogue rock avalanche deposits: a kinematic analysis of the propagation mechanism

C. Longchamp[1], A. Abellan[1], M. Jaboyedoff[1], and I. Manzella[2]

[1]Institute of Earth Sciences, University of Lausanne, Lausanne, Switzerland
[2]Department of Earth Sciences, University of Geneva, Geneva, Switzerland

Received: 22 October 2015 – Accepted: 27 October 2015 – Published: 10 November 2015

Correspondence to: C. Longchamp (celine.longchamp@unil.ch)

Published by Copernicus Publications on behalf of the European Geosciences Union.

Abstract

Rock avalanches are extremely destructive and uncontrollable events that involve a great volume of material ($> 10^6$ m^3), several complex processes and they are difficult to witness. For this reason the study of these phenomena using analogue modelling and the accurate analysis of deposit structures and features of laboratory data and historic events become of great importance in the understanding of their behavior.

The main objective of this research is to analyze rock avalanche dynamics by means of a detailed structural analysis of the deposits coming from data of 3-D measurements of mass movements of different magnitudes, from decimeter level scale laboratory experiments to well-studied rock avalanches of several square kilometers magnitude.

Laboratory experiments were performed on a tilting plane on which a certain amount of a well-defined granular material is released, propagates and finally stops on a horizontal surface. The 3-D geometrical model of the deposit is then obtained using either a scan made with a 3-D digitizer (Konica Minolta vivid 9i) either using a photogrammetric method called Structure-from-Motion (SfM) which requires taking several pictures from different point of view of the object to be modeled.

In order to emphasize and better detect the fault structures present in the deposits, we applied a median filter with different moving windows sizes (from 3×3 to 9×9 nearest neighbors) to the 3-D datasets and a gradient operator along the direction of propagation.

The application of these filters on the datasets results in: (1) a precise mapping of the longitudinal and transversal displacement features observed at the surface of the deposits; and (2) a more accurate interpretation of the relative movements along the deposit (i.e. normal, strike-slip, inverse faults) by using cross-sections. Results shows how the use of filtering techniques reveal disguised features in the original point cloud and that similar displacement patterns are observable both in the laboratory simulation and in the real scale avalanche, regardless the size of the avalanche. Furthermore, we observed how different structural features including transversal fractures and folding

patterns tend to show a constant wavelength proportional to the size of the avalanche event.

1 Introduction

Rock avalanches, or Sturzstroms (Heim, 1932) are defined as an extremely rapid, massive, flow-like motion of fragmented rocks derived from a bed-rock failure (Hungr et al., 2001). Rock avalanches are events in which granular masses of rock debris flow at high speeds, commonly with unusually runout (Corominas, 1996; Friedmann and Losert, 2003). A great volume of material ($> 10^6\,m^3$) is involved and the flowing mass can reach velocities in the order of tens meters per second. They can travel long distances, in the order of kilometers and cover an area over $0.1\,km^2$ (Hsü, 1975). They present a very high mobility and need to be simulated with adapted frictional models (Hungr et al., 2001; Pedrazzini et al., 2012). Authors proposed different possible causes, which could explain the high mobility of these phenomena, such as the influence of the large destabilized volume (Heim, 1932; Hsü, 1975; Scheidegger, 1973; Nicoletti and Sorriso-Valvo, 1991), the momentum transfer within the rear and the front of the flowing mass (Van Gassen and Cruden, 1989; Manzella and Labiouse, 2009), or the fragmentation of the spreading mass (Heim, 1932; Davies, 1982; Davies and McSaveney, 1999; Locat et al., 2006). In order to understand the behavior of such granular flows, laboratory scale experiments provide important information on their propagation and on the parameters influencing their mobility, even if they reproduce idealized conditions (Davies and McSaveney, 1999, 2003; McDougall and Hungr, 2004; Shea and van Wyk de Vries, 2008; Manzella and Labiouse, 2008, 2009). Several authors proposed different parameters for the geometrical description of large landslides. One of the most used is the Fahrböschung concept, which was introduced by Heim (1932) to estimate the maximum runout of rock avalanches or landslides (Scheidegger, 1973; Hsü, 1975; Davies, 1982) and which is defined as the angle of the straight line connecting the head of the scar to the end of the deposit.

ESURFD
3, 1255–1288, 2015

Analysis of analogue rock avalanche deposits

C. Longchamp et al.

The presence of faults and folds are common features on the surface of rock-avalanche deposits. One of the best examples is the rock avalanche deposit of Socompa volcano (Northern Chili). This deposit was widely studied before (Francis et al., 1985; van Wyk de Vries et al., 2001; Kelfoun and Druitt, 2005; Shea and van Wyk de Vries, 2008) and presents a well preserved morphology thanks to the local arid climate. A complex assemblage of surface structures (normal faults, strike-slip faults, thrusts, ridges) is displayed on the surface of the deposit. Van Wyk de Vries et al. (2001) showed that these structures incise deeply the internal part of the deposit. The non-volcanic deposit of Blackhawk (California, USA) also presents similar features (Shea and van Wyk de Vries, 2008) (Fig. 1a) as well as the Frank Slide in Alberta (Canada) (Cruden and Hugr, 1986, 2011; Charrière et al., 2015). Features perpendicular to the flow direction are mainly present in the distal part of the deposit and are interpreted as the surface expression of the underneath topography. Reversibly, longitudinal features on the proximal and the central part of the deposit are assumed to be morphological features that were created during the process of avalanche propagation and deposition. It is also interesting to highlight that similar features have been observed in other planets such as in the Mont Olympus (Mars) (Fig. 1b). Shea and van Wyk de Vries (2008) provided a detailed map of this extraterrestrial Martian rockslide avalanche where it can be observed that thrust faults are located in the front of the deposit and that are cut by strike-slip faults. Normal faults are presented in the central part of the deposit. Although, these features occur during the emplacement of the deposit, however, few studies focus on these deformational settings.

In the present paper a detailed structural analysis is carried out based on data coming from dedicated laboratory experiments and historic events in order to better understand the dynamics of these complex phenomena.

ESURFD
3, 1255–1288, 2015

2 Data acquisition

The first step of this study consisted in carrying out laboratory experiments in order to study the influence of a series of parameters on the features and structure of granular flow deposits. The experimental setup (see Fig. 2) consisted in a simple aluminium slope geometry composed of two distinct parts: a 90 cm × 70 cm slope with an inclination (α) which can be precisely modified, connected with a curved part to a 120 cm long horizontal surface. Furthermore, the experimental setup also includes a box (11 cm × 8 cm × 7 cm) where the loose material is enclosed at the beginning of the experiment. This box, separated from the main set-up, can be leant against the slope and quickly separated from it by means of a retractile jack. This allows placing a precise quantity of granular material on the slope and realising it avoiding any vibrations. Experiments then consist letting the mass propagating without lateral confinements till it reaches a complete stop (Fig. 2).

Two different materials were used for the experiments: (a) the first type of material corresponds to angular and calibrated carborandum sand (SiC, density = 3.21 g cm^{-3}) with three different grainsizes (Table 1). The choice of carborandum was made in order to avoid the characteristic electrostatic effects that have been often observed in granular flow experiments and that are not present in real events (Iverson and Denlinger, 2001; Manzella, 2008). Furthermore, the angular shape of this type of material has close resemblances with natural material, (b) the second material corresponds to colored sands of similar grainsize. The choice of this material was driven by the need of observing the evolution of the initial stratigraphy, i.e. to analyze the deposit stratigraphy (given by different layers of different colors) during motion and emplacement of the mass.

The slope and the surface of deposition were artificially roughed by adding sandpaper, also made of carborandum sand, where the grain diameter has been varied. The basal roughness Ra has been deduced according to the formula of Adams et al. (2012)

ESURFD
3, 1255–1288, 2015

and shown in Eq. (1):

$$\varepsilon = 5.863\,\mathrm{Ra} \tag{1}$$

where Ra [µm] is the roughness of a hypothetical surface assumed to be made of a uniform monolayer of spheres having the same mean diameter ε [µm].

Based on Eq. (1), the basal roughness Ra can be calculated as follow (Eq. 2):

$$\mathrm{Ra} = \frac{\varepsilon}{5.863} \tag{2}$$

The basal roughness Ra varied between 45.88 µm (ε = 269 µm) (for the coarser sandpaper) and 1.43 µm (ε = 8.4 µm) (for the finer sandpaper) to obtain six different substrata (Table 2). All the experiments were carried out with a constant volume within the same experiment ($400\,\mathrm{cm}^3 < V < 500\,\mathrm{cm}^3$), same slope angle (40°) and same height of fall for the granular material. The experiments were recorded by a high speed camera, the final deposit was scanned by a 3-D digitizer (Konica Minolta vivid 9i micro-Lidar, Fig. 2) and photographed. Finally a transparent separation is placed carefully along the major longitudinal section and the material on one side is removed so that it is possible to observe the internal structure of the mass. In order to observe the repartition of the colored sand grains within the deposit, sand grains were counted at crucial sections along the deposit. For each measurement, a section of 0.2 cm length and a height corresponding to the thickness of the deposit was determined. Into this section, the number of colored grains were manually counted Ten measurements were made along the deposit and cumulated.

In order to have significant results, three experiments are carried out with equal initial conditions.

3 Methodology

As mentioned above, during the propagation, the motion of the granular mass is recorded by a high-speed camera in order to analyze the deformation and spreading during the flow. Once the mass stopped, the first step was to take pictures of the deposit in order to study and inventory the visible longitudinal and transversal features on the surface. The acquisition of 3-D dataset was made using either a laser scanner (Konica Minolta vivid 9i micro-Lidar) either a photogrammetry technique, named Structure-from-Motion (SfM) (Westboy, 2012). The laser scanner technique is useful to scan the deposit resulting of the propagation of carborandum sand but the density of points is quite low (30 000 points per point cloud) (see Fig. 3b). Moreover, the setup is quite difficult to install and the data are long to process. SfM differs fundamentally from conventional photogrammetry, in that the geometry of the scene, camera positions and orientation is solved automatically without the need to specify a priori a network of targets which have known 3-D positions (Westboy, 2012). Instead, these parameters are solved simultaneously using a highly redundant, iterative bundle adjustment procedure, based on a database of features automatically extracted from a set of multiple overlapping images (Westboy, 2012). Structure from Motion is a simple technique requiring little material. The density of points is high (1 000 000 points per point cloud). This density of points allows identifying finer features on the deposit. The main disadvantage of this technique is that the post processing of the data is sensitive to all variation in the images. Therefore, SfM cannot be applied to experiments with carborandum sand as the grains reflect the light with different intensity according to where the pictures is taken and it could only be applied to the colorized sand deposit (Fig. 4). Thanks to the use of different filtering techniques and operators, we were able to highlight the structural fingerprints on the deposit surface. This computational work aimed to highlight the features that cannot be observed by a naked eye, as follow.

3.1 Application of a median filter technique

Data acquisition using 3-D digitizer leads or SfM to a "noisy" surface in which the features to be detected are masked due to the scattering of the 3-D points around the real surface (Fig. 5a). To remove the noise, smoothing filters are used in preprocessing steps (Gonzalez and Woods, 2002; Pugazhenti and Priya, 2013). After Gonzalez and

Woods (2002), order-statistic filters are nonlinear filters whose response is based on ordering the pixel contained in the image area encompassed by the filter, and then replacing the value of the center pixel with the value determined by the ranking value. The first step was to remove the noise using a 2-D median filtering using different window sizes (Fig. 5b and c).

3.2 Application of a gradient operator

Once the noise was removed of the dataset obtained with 3-D digitizer or SfM, a numerical gradient is applied to the filtered dataset. The gradient was applied along two directions to highlight changes in the slope orientation as proposed in Kumar et al. (1996) and Gonzalez and Woods (2002). First, we calculated the gradient parallel to the flow direction (along the x axis), and then the gradient perpendicular to the flow direction (along the y axis):

$$\nabla F = \frac{\partial F}{\partial x} i + \frac{\partial F}{\partial y} j \quad (3)$$

The objective of detecting variation of the gradient along x and y is to highlight any preferential orientation. The detected variations of the slope are interpreted as structures developed on the surface of the deposit. Once the gradient operator is applied, the point cloud is imported in the IMInspect module of Polyworks software (InnovMetric).

3.3 Comparison with real case

In order to extend the proposed workflow to a real case study, we decided to apply the filtering gradient operator techniques to the well-known Frank Slide event (Alberta, Canada). This deposit presents several geometrical features, which are mainly longitudinal and perpendicular to the flow direction (Longchamp et al., 2011; Charrière et al., 2015).

ESURFD
3, 1255–1288, 2015
Analysis of analogue rock avalanche deposits
C. Longchamp et al.

4 Results

4.1 Results I: experiment description

4.1.1 Visual inspection from photography

Laboratory experiments were carried out with different volumes, grainsizes and using different basal roughness but only the finer grainsize (F120) presented visible features on the surface of the deposit as shown in Fig. 6a. Three distinct sets of features can be observed in this figure: inverse faults, normal faults and strike-slip faults. The first set, the inverse faults, is composed of long features, perpendicular to flow direction following the outline of the front with a tendency to become parallel to the global flow direction at the lateral margins (green lines on Fig. 6b). The second set is formed by thin normal faults located at the rear part of the deposit and perpendicular to the flow direction (red lines on Fig. 6b). Two different sets of strike-slip faults can be observed. The first one is composed of short and thin features parallel to the flow direction and present at the front of the deposit. These features can be observed cutting the inverse faults at the frontal part and cutting the normal faults at the rear part. The second one is made of strike-slip faults parallel to the flow direction and are present at the lateral margins of the deposit.

4.1.2 Visual inspection from high speed video

In high-speed video, propagation of the mass is easily observable. Sand of three different colors was used and was poured in the starting box as follow: 150 mL of red sand as the lower layer, 150 mL of grey sand as intermediate layer and finally, 150 mL of green sand. The slope is made rough with the finer substratum (Ra = 1.43 µm) and the slope angle is 40°. Once the trap is open and the material is free to flow, all the layers are stretched under an extensional regime. Once the frontal part reach the horizontal surface, its velocity is decreased. As the mass continues to flow on the slope, the front

ESURFD
3, 1255–1288, 2015

is compressed and pushed forward. The mass is finally stopped once all the mass reaches the horizontal surface. The high-speed video is available in the Supplement.

4.2 Results II: point cloud processing

Figure 7 shows the results of the point cloud processing for all the simulations, i.e. using three grainsizes (F10, F36 and F120) on the different substrata (Table 2). For the coarser grainsize (F10), the application of the different filters and operator techniques has not highlighted any remarkable features. The only noticeable thing is that the shape of the deposit became more ellipsoidal with a decreasing basal roughness. For the medium grainsize (F36) the filters clearly highlighted a series of features perpendicular to the flow direction. The density of these features increases with the reduction of the basal roughness. In this case filters allowed detecting features that were not visible on the pictures alone.

As it can be observed on Fig. 7, the gradient along Y can be considered as an efficient manner for the observation of the different features affecting the surface of the deposits.

Using this operator, we observed that the back of the deposit presents high concentration of small features parallel to the flow direction. Figure 8a and b presents the back of an analogue deposit (F120 on the finest substratum, Ra = 1.43 µm) after the point cloud processing and imported in the IMInspect module of Polyworks software (InnovMetric). Two different sets are observable: one perpendicular to the flow direction and the second composed of features parallel to the flow direction and cutting the first set (Fig. 8). The first set was observed with naked eye whereas the second set is only recognizable after post processing.

4.3 Frank Slide

The same visual inspection and filtering methods were applied to the Frank Slide deposit. Figure 9a is the result of the interpretation of the features mapped directly on the

ESURFD

3, 1255–1288, 2015

DEM and Fig. 9b is the result of the application of a gradient along the flow direction. The main features observed in the DEM are also recognizable on the gradient map, but a series of structures that are masked on the DEM image can be identified in the gradient image. Figure 9c and d shows a zoom of the deposit after the filtering. In the Fig. 9c, features parallel to the flow direction are clearly identifiable whereas in the Fig. 9d, the features are parallel to the flow direction.

5 Discussion

Our workflow has allowed the identification of three distinct sets of features on the analogue granular flow deposit. Those features are important marks of the processes happening during the flow and the emplacement of the mass and could be crucial in improving our understanding of the dynamics and the reasons of the high mobility of rock avalanches. The inverse faults are well marked on the deposit front, reflecting the compression affecting the frontal part of the mass. Inverse faulting system appears as soon as the frontal part of the granular mass hits the surface of deposition and its velocity starts to slow down. Then, the granular material accumulates on the rear part, pushing forward and compressing the frontal part of the deposit. Normal faults were formed during an extensional regime, when the mass was stretched during the flow and by the pulling of the frontal part of the mass. Strike-slip faults are present at the front of the deposit. As the mass is thinner at the margins and consequently the velocity decreases while the central part of the mass is still on motion letting strike-slip faults appear at the lateral margins of the deposit. The strike-slip faults are the expression of the shearing occurred during the deceleration of the mass (Shea and van Wyk de Vries, 2008).

Thanks to the application of the filtering on analogue deposit 3-D datasets, the structures observed during the laboratory experiments were highlighted. One advantage is that the use of filters allows detecting features for the finest sand (F120) and also for the medium one (F36), for the totality of the basal roughness. The fact that no features are observed for the coarse grainsize (F10) can be explained by the fact that the size of features is of the same order of magnitude that the size of the grains. The gradient along Y gave the best results since it allowed detecting long inverse faults at the front and some normal faults at the back. Moreover, the study of the result of the Y gradient with the Polyworks software shows that the normal faults at the back are numerous and cut by strike-slip faults (Fig. 8). These strike-slips faults appear after the extensional regime, during the shearing caused by the mass deceleration. These features give crucial information for the mobility of the mass and are not detectable with naked eye.

Thus, different regimes were distinguished: the compressional, the extensional and the shearing regimes. Based on this assumption we could deduce the behavior of the granular mass looking at the high-speed camera snapshots as shown in Fig. 10. This figure represents for each time step on one side the movie snapshot and on the other the interpretation related to it. In order to improve the clarity of the observation made, no distinction between the layers is made for the interpretation. Two main regimes are detected, the compressional, outlined on the interpretation with dots and the extensional one, outlined with lines. Following the time steps shown in Fig. 10 we can then observe:

Step 1: Once the trap is open, the front of the granular material starts to flow.

Step 2: All the mass behaves under an extensional regime through all directions during the time preceding the deposition of the granular flow.

Step 3: Shortly after the free flow, the front of the mass hits the surface of deposition, decreasing suddenly its velocity. Two different tensional states are found at this step. While the mass on the slope it is under high extensional regime the front starts to be under compressional regime as it hits the surface of deposition and the velocity starts to slow down. In addition to that, at this stage of the experiment, we start observing one additional aspect characterizing the green layer. In fact we can first distinguish a part of the green mass flowing which behaves differently from the rest of the mass. This part is likely to constitute the rear zone in the initial configuration of this layer. Moreover, at this step, it can be observed that the basal red layer has a lower velocity than the other layers, as it is less visible in the picture.

Step 4: At this step, the back is still under an extensional regime and the front under a high compressive regime as the flowing material continues to push it forward. The rear part of the green layer is faster than the underneath layers.

Step 5: The gray and green layers continue to be pushed by the main body of the mass. Consequently, shearing appears at the front. As the red layer is the basal layer, it is slowed by friction. As the margins of the mass are thinner compared to the central part, their velocity is less important and shearing takes place. Simultaneously, the rear part of the green layer is faster compare to the lower layers and hits the mass already deposited.

Step 6: The back of the mass continues to flow and is still under extensional regime, pushing the front forward. At this step, shearing is still important at the margins and at the front.

Step 7: The front is stopped and the rest of the material still on the ramp finishes to flow down creating the shearing observed at the back of the deposit, cutting the normal faults.

Step 8: The mass is finally stopped. It is interesting to highlight that the original stratigraphy is conserved and observable at the front.

The profile AA′ along the flow direction was obtained for the laboratory experiment (Fig. 11a). This profile allowed observing the internal part of the mass and the depth of the main features. Figure 11b gives the image of the section along the AA′ line shown in Fig. 11a and the Fig. 11c is its interpretation. In Fig. 11c, inverse faults are visible at the front (well-marked by red grains in the Fig. 11b) whereas normal faults are visible

Discussion Paper | Discussion Paper | Discussion Paper | Discussion Paper |

ESURFD

3, 1255–1288, 2015

Analysis of analogue rock avalanche deposits

C. Longchamp et al.

at the rear part of the deposit. In this figure, it can be observed that the center of the mass is mainly composed of green sand, confirming that the rear part of the green layer in Fig. 10 hits the mass already present on the surface of deposition (steps 5–7 in Fig. 10). When this mass hits the deposit, it probably increased the compression explaining the numerous inverse faults present at the front (Fig. 11c).

To confirm what observed the number of colored sand grains has been counted along the central section of the deposit, as reported on Fig. 12. Results confirmed what showed by Fig. 11b and c with the identification of an extension-dominated area in the rear and a compression dominated area in the front. The rear part of the deposit corresponds to the extension-dominated area. This area is mainly composed of red sand whereas few green grains were observed. In the contrary, the central part of the deposit is mainly composed of green sands. Indeed, this part corresponds to the rear part of the deposit that hit the mass already deposited (Fig. 10). The frontal part of the deposit corresponds to the compression-dominated area. The compression caused by the impact of the green layer of grains in the central part pushed part of the lower layer (red) further on the front and towards the surface creating the inverse faults also showed in Fig. 11c. Indeed, in this frontal part, we can observe that the amount of red sand increases.

Because of the position of the profile, the red layer is not clearly visible at the front of Fig. 11b and c but the conservation of the initial stratigraphy is observable in the Fig. 11a. The fact that the initial stratigraphy is preserved in the final deposit it is relevant since this feature has been already detected in several real cases and it has been recognized as one of the main ones characterizing rock avalanche deposit (Erismann, 1979; Manzella and Labiouse, 2013). Thanks to the film analysis we could then relate some propagation mechanisms with the consequent preservation of the initial stratigraphy in the final deposit and this could give an insight in the dynamics of real rock avalanches.

Based on these observations, we can propose a mechanism of propagation of a granular flow as shown in Fig. 13 and explained in the following:

ESURFD

3, 1255–1288, 2015

1. The granular material is released and the extension of the mass starts immediately when the mass starts to flow. When the mass flows freely on the slope, the velocity of the front is assumed to be similar to the velocity observed at the back of the moving mass (Shae and van Wyk de Vries, 2008).
2. When the front of the mass hits the horizontal surface, a compressional regime appears at the front while the mass on the slope is under high extensional regime. The frontal part of the deposit is stopped and then, pushed forward by the mass remaining on the slope; thus the first inverse faults appear at the front.
3. Although the frontal part of the deposit is slowed down, the mass continues to propagate on the surface of deposition; thus the front is under a high compressional regime leading to the generation of several inverse faults. Furthermore, shearing takes place at the margins of the deposit, generating strike-slip faults. The rear part of the granular flow is still descending along the slope where normal faults are forming because of the extensional state.
4. Now the mass is completely on the horizontal surface and a thickening of the main body is observe. The moving forward of the mass imply the extension of the back and the formation of normal faults whereas the font is still compressed. The shearing results from the deceleration of the mass.
5. The mass continues to decelerate on the horizontal surface, the strike-slip faults appear at the front of the deposit. These strike-slip faults cut both the invers and the normal faults. This type of features is the latest features that appear during all the process of the propagation; they are caused by the progressive deceleration of the mass. Strike-slip faults are the surface expression of the shearing at the base of the deposit occurring while the mass is ceasing its movement.
6. The mass has come to a complete stop.

Based on this mechanism of propagation, we understand why the features are not randomly exposed at the surface of the deposit. As it can be observed in Fig. 6, the

ESURFD
3, 1255–1288, 2015

inverse faults are present a the frontal part of the deposit, which correspond to the compression-dominated area. Normal faults are mainly observed at the back of the deposit (Figs. 6 and 8), which correspond to the extension-dominated area. Finally, strike-slipe faults are observed at the back and at the margins of the deposit (Figs. 6 and 8). These repartition was also observed in the Blackhawk deposit (Fig. 1a) and in a Martian deposit (Fig. 1b) (Shea and van Wyk de Vries, 2008). Based on the study of the DEM of Frank Slide deposit and with the filtering thechniqu, the same repartition of the features was observed (Fig. 9).

6 Conclusions

The use of 3-D dataset, accurate visual inspection and a performing filtering method give crucial information on the motion of granular mass. To summarized:

1. Three families of faults were highlighted on the surface of the deposit: normal faults, inverse faults and strike-slip faults. We also highlighted that strike-slip faults are present at the back of the deposit.

2. The identification of the different features allowed identifying three regimes during the propagation of the mass: extensional, compressional and shearing. The extension to real cases of the interpretation of the motion of the granular mass based on laboratory experiments is comforted by the fact that the initial stratigraphy is preserved in both cases and this is an important characteristic of rock avalanche deposits.

3. The result of the filters on the 3-D dataset is a colored point cloud were the slope variations are assigned to a color scale. The method is fast and results into a rapid mapping of the deposit.

4. The use of laser scanner and Structure from Motion are two different techniques to get 3-D dataset. Both are valid and often they result to be complementary.

ESURFD
3, 1255–1288, 2015

5. The analogue deposits present similar features as real cases events (Blackhawk and Martian deposits, Fig. 1).

The application of the filtering technique on the deposit of the Frank Slide rock avalanches gives encouraging results and after some further improvements could be applied in the future to understand the dynamics of emplacement of historic rock avalanche observing interpreting their deposit features.

The Supplement related to this article is available online at doi:10.5194/-15-1255-2015-supplement.

Acknowledgements. The authors are grateful to P.-E. Cherix for the design of the laboratory setup and to the Alberta Geological Service for providing the data of the Frank Slide.

References

Adams, T., Grant, C., and Watson, H.: Simple algorithm to relate surface roughness to equivalent sand grain roughness, Int. J. of Mechnical Engineering and Mechatronics, 1, 2929–2724, 2012.

Charrière, M., Humair, F., Froese, C., Jaboyedoff, M., Pedrazzini, A., and Longchamp. C.: From the source area to the deposit: collapse, fragmentation and propagation of the Frank Slide, GSA Bull., B31243.1, 1–21, 2015.

Cruden, D. M. and Hungr, O.: The debris of the Frank Slide and theories of rockSlide-avalanche mobility, Can. J. Earth Sci., 23, 425–432, 1986.

Davies, T. R.: Spreading of rock avalanche debris by mechanical fluidization, Rock Mech., 15, 9–24, 1982.

Davies, T. R. H. and McSaveney, M. J.: Runout of dry granular avalanches, Can. Geotech. J., 36, 313–320, 1999.

Davies, T. R. H. and McSaveney, M. J.: Runout of rock avalanches and volcanic debris avalanches, Proc. Int. Conf. on Fast Slope Movements, 11–13 May 2003, Vol. 2 Naples, Italy, 2, 2003.

Erismann, T. H.: Mechanisms of large landslides, Rock Mech. Felsmechanik, 12, 15–46, 1979.
Francis, P. W., Gardeweg, M., O'Callaghan, L. J., Ramirez, C. F., and Rothery, D. A.: Catastrophic debris avalanche deposit of Socompa volcano, north Chile, Geology, 14, 600–603, 1985.
Friedman, S. J., Kwon, G., and Losert, W.: Granular memory and its effect on the triggering and distribution of rock avalanche events, J. of Geophys. Res., 108, 1–11, 2003.
Gonzalez, R. C. and Woods, R. E.: Digital Image Processing – Sec. Ed., Prentice-Hall Inc., Upper Saddle River, New Jersey, USA, 190 pp., 2002.
Heim, A.: Der Bergsturz und Menschenleben, Fretz und Wasmuth Verlag, Zürich, Switzerland, 218 pp., 1932.
Hsü, K. J.: Catastrophic debris streams (strurzstroms) generated by rockfall, Geol. Soc. Am. Bull., 86, 129–140, 1975.
Hungr, O., Evans, S. G., Bovis, M., and Hutchinson, J. N.: Review of the classification of landslides of the flow type, Environ. Eng. Geosci., VII, 221–238, 2001.
Iverson, R. M. and Denlinger, R. P.: Flow of variably fluidized granular masses across three-dimensional terrain I. Coulomb mixture theory, J. Geophys. Res.-Sol. Ea., 106, 537–552, 2001.
Kelfoun, K. and Druitt, T. H.: Numerical modelling of the emplacement of Socompa rock avalanche, Chile, J. Geophys. Res., 110, B12202, doi:10.1029/2005JB003758, 2005.
Kumar, L., Skidmore, A. K., and Knowles, E.: Modelling topographic variation in solar radiation in a GIS environment, Int. J. Geo. Information Sc., 11, 475–497, 1996.
Locat, P., Couture, R., Leroueil, S., Locat, J., and Jaboyedoff, M.: Fragmentation energy in rock avalanches, Can. Geotech. J., 43, 830–851, 2006.
Longchamp, C., Charrière, M., and Jaboyedoff, M.: Experiments on substratum roughness, grainsize and volume influence on the motion and spreading of rock avalanches, Pan-Am CGS Geotechnical Conference, 2–6 October 2001, Toronto, Ontario, Canada, 2001.
Manzella, I.: Dry rock avalanche propagation: unconstrained flow experiments with granular materials and blocks at small scall, Ph.D thesis, Ecole Polytechnique Fédérale de Lausanne, 2008.
Manzella, I. and Labiouse, V.: Qualitative analysis of rock avalanches propagation by means of physical modelling of not constrained gravel flows, Rock Mech. Rock Eng., 41, 133–151, 2008.

ESURFD
3, 1255–1288, 2015

Analysis of analogue rock avalanche deposits

C. Longchamp et al.

Manzella, I. and Labiouse, V.: Flow experiments with gravel and blocks at small scale to investigate parameters and mechanisms involved in rock avalanches, Eng. Geol., 109, 146–158, 2009.
Manzella, I. and Labiouse, V.: Empirical and analytical analyses of laboratory granular flows to investigate rock avalanche propagation, Landslides, 10, 23–36, 2013.
McDougall, S. and Hungr, O.: A model for the analysis of rapid landslide motion across three-dimensional terrain, Can. Geotech. J., 41, 1084–1097, 2004.
Nicoletti, P. G. and Sorriso-Valvo, M.: Geomorphic controls of the shape and mobility of rock avalanches, Geol. Soc. Am. Bull., 103, 1365–1373, 1991.
Pedrazzini, A., Froese, C. R., Jaboyedoff, M., Hungr, O., and Humair, F.: Combining digital elevation model analysis and run-out modeling to characterize hazard posed by a potentially unstable rock slope at Turtle Mountain, Alberta, Canada. Eng. Geol., 128, 76–94, 2012.
Pugazhenti, D. and Pria, K.: A quantitative approach for textural image segmentation with median filter, Int. J. of Advancements in Res. & Tech., 2, 179–183, 2007.
Scheidegger, A. E.: On the prediction of the reach and velocity of catastrophic landslides, Rock Mech. Rock Eng., 5, 231–236, 1973.
Shea, T. and van Wyk de Vries, B.: Structural analysis and analogue modeling of the kinematics and dynamics of rockslide avalanches, Geosphere, 4, 657–686, 2008.
Van Gassen, W. and Cruden, D. M.: Momentum transfer and friction in the debris of rock avalanches, Can. Geotech. J., 26, 623–628, 1989.
van Wyk de Vries, B., Self, S., Francis, P. W., and Keszthelyi, L: A gravitational spreading origin for the Socompa debris avalanche, J. Volcanol. Geoth. Res., 105, 225–247, 2001.
Westboy, M. J., Brasington, J., Glasser, N. F., Hambrey, M. J., and Reynolds, J. M.: “Structure-from-Motion” photogrammetry: a low-cost, effective tool for geoscience applications, Geomorphology, 179, 300–314, 2012.

ESURFD
3, 1255–1288, 2015

Table 1. Characteristics of the used material.

Grading		Mean grainsize (µm)	Range (µm)
Coarse	F10	2605	2830–2380
Medium	F36	545	590–500
Fine	F120	115	125–105
Colored	–	500	–

ESURFD

3, 1255–1288, 2015

Table 2. Characteristics of the different substrata.

Grading	Grit	Grainsize (µm)	Ra (µm)
Coarse	60	269	45.88
	120	125	21.32
Medium	320	46.2	7.88
	600	25.8	4.40
Fine	1200	15.3	2.61
	2500	8.4	1.43

ESURFD

3, 1255–1288, 2015

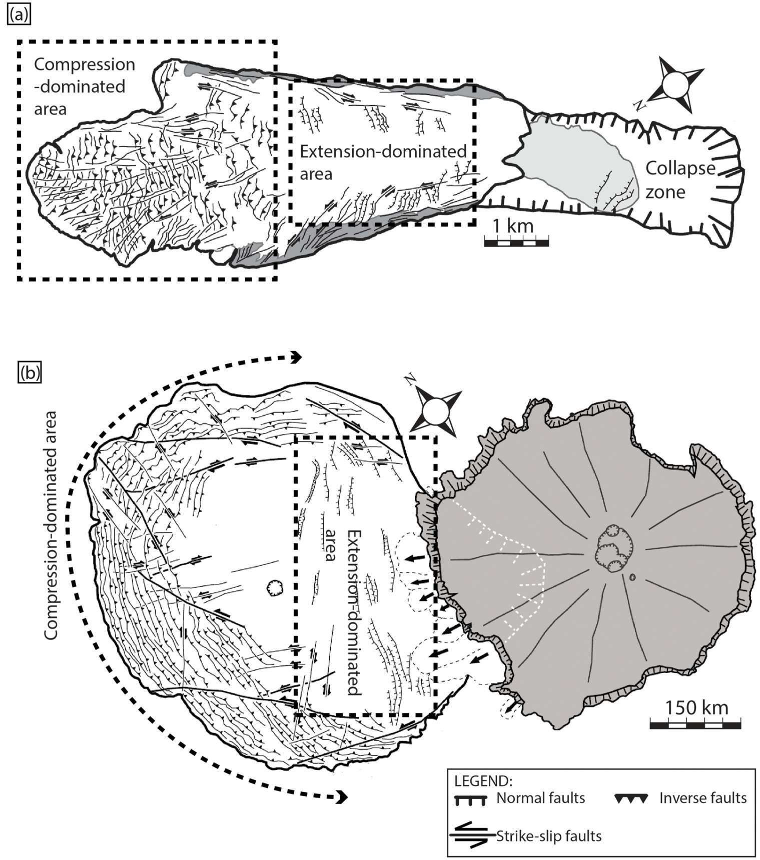

Figure 1. (a) Blackhawk deposit and **(b)** Martian deposit (modified after Shea and van Wyk de Vries, 2008).

ESURFD

3, 1255–1288, 2015

Analysis of analogue rock avalanche deposits

C. Longchamp et al.

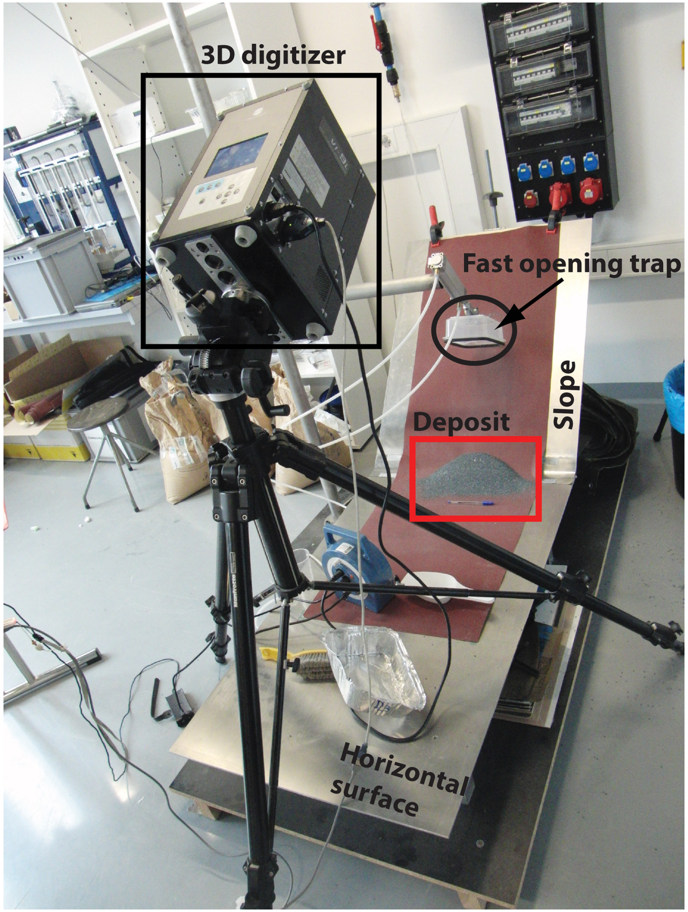

Figure 2. Laboratory setup.

ESURFD
3, 1255–1288, 2015

Title Page
Abstract | Introduction
Conclusions | References
Tables | Figures
Back | Close
Full Screen / Esc
Printer-friendly Version
Interactive Discussion

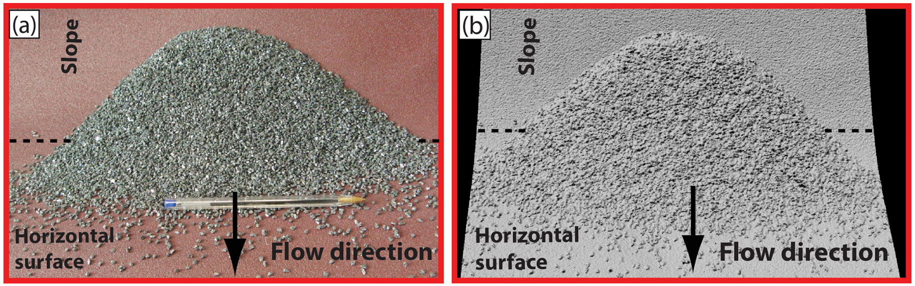

Figure 3. (a) Photography of a deposit of coarse granular material; **(b)** 3-D model of the deposit obtained by 3-D laser scanning (red square in Fig. 2).

ESURFD
3, 1255–1288, 2015

Analysis of analogue rock avalanche deposits

C. Longchamp et al.

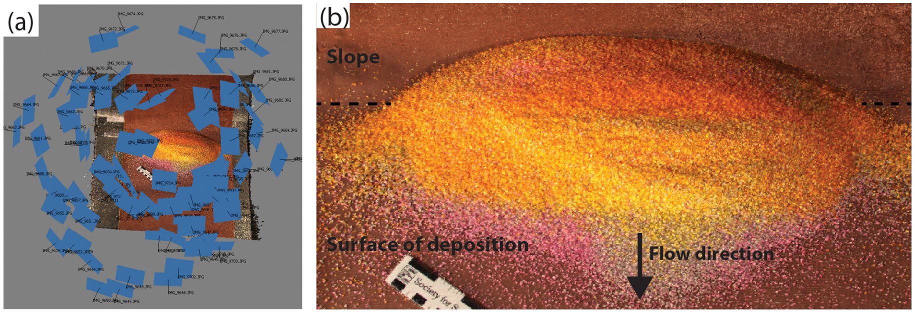

Figure 4. (a) View of the different position of the camera to take pictures for structure-from-motion; **(b)** 3-D model obtained with structure-from-motion. Three colored sands were used for this experiment (yellow, grey, pink).

ESURFD
3, 1255–1288, 2015

Analysis of analogue rock avalanche deposits

C. Longchamp et al.

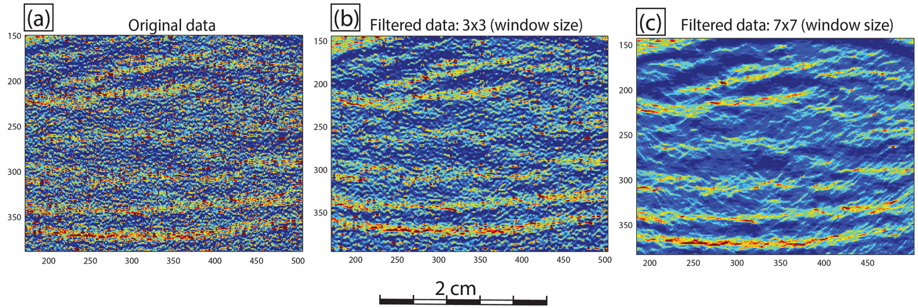

Figure 5. Application of the median filter to remove noises. **(a)** Original data; **(b)** filtered data; **(c)** with a 3 × 3 window size; **(d)** filtered data with a 7 × 7 window size.

ESURFD
3, 1255–1288, 2015

Analysis of analogue rock avalanche deposits

C. Longchamp et al.

Title Page
Abstract Introduction
Conclusions References
Tables Figures
◄ ►
Back Close
Full Screen / Esc
Printer-friendly Version
Interactive Discussion

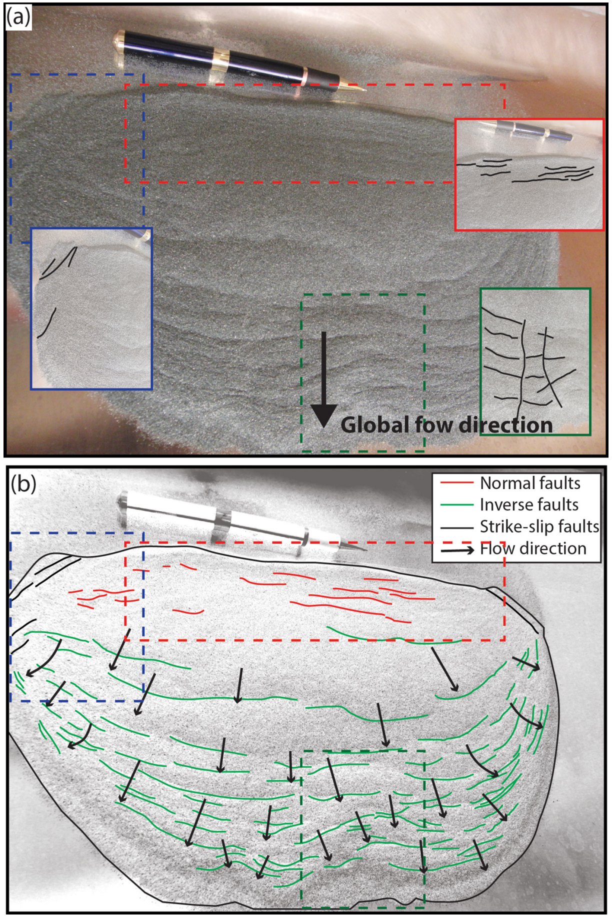

Figure 6. (a) analogue deposit (F120, aluminum substratum), view from the top; **(b)** result visual inspection and features mapping observed on the deposit surface.

ESURFD
3, 1255–1288, 2015

Analysis of analogue rock avalanche deposits

C. Longchamp et al.

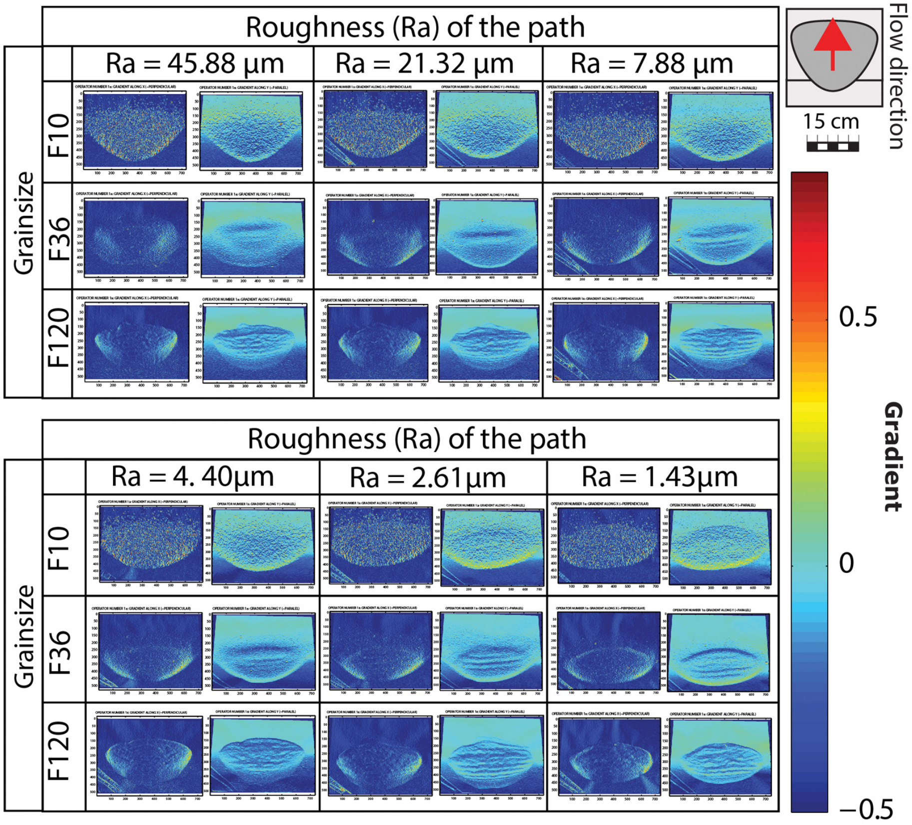

Figure 7. Results of the gradient along X and Y applied to all experiments carried for this research. The best results are obtained with the gradient along Y. The influence of the grainsize and the substratum on the shape of the deposit is clearly observable.

ESURFD
3, 1255–1288, 2015

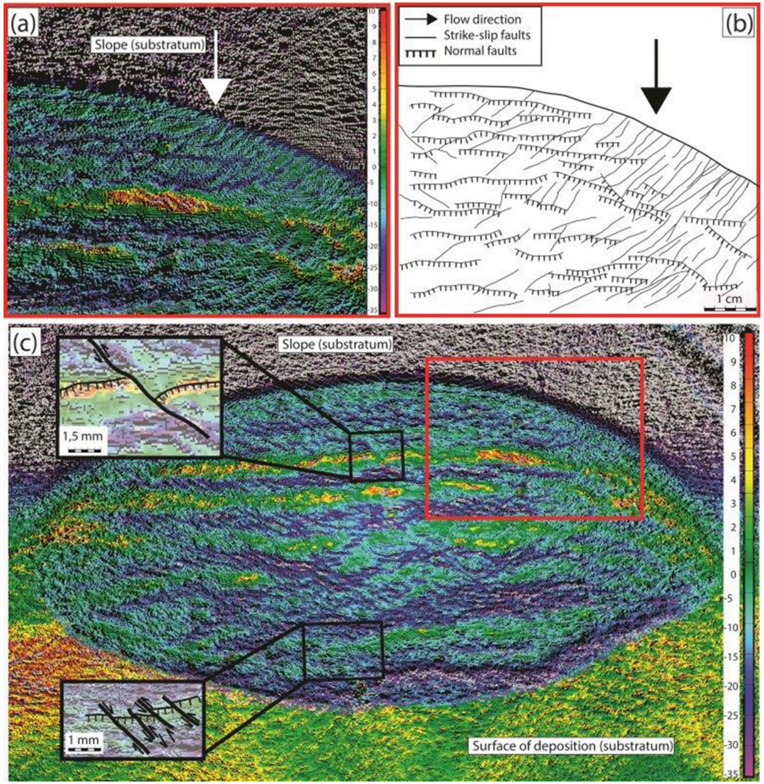

Figure 8. (a) Portion of the back of a deposit after post-processing and **(b)** detailed mapping of the back of the deposit. Strike-slip faults are numerous at the back, cutting normal faults. **(c)** the whole result.

ESURFD
3, 1255–1288, 2015

Analysis of analogue rock avalanche deposits

C. Longchamp et al.

ESURFD
3, 1255–1288, 2015

Analysis of analogue rock avalanche deposits

C. Longchamp et al.

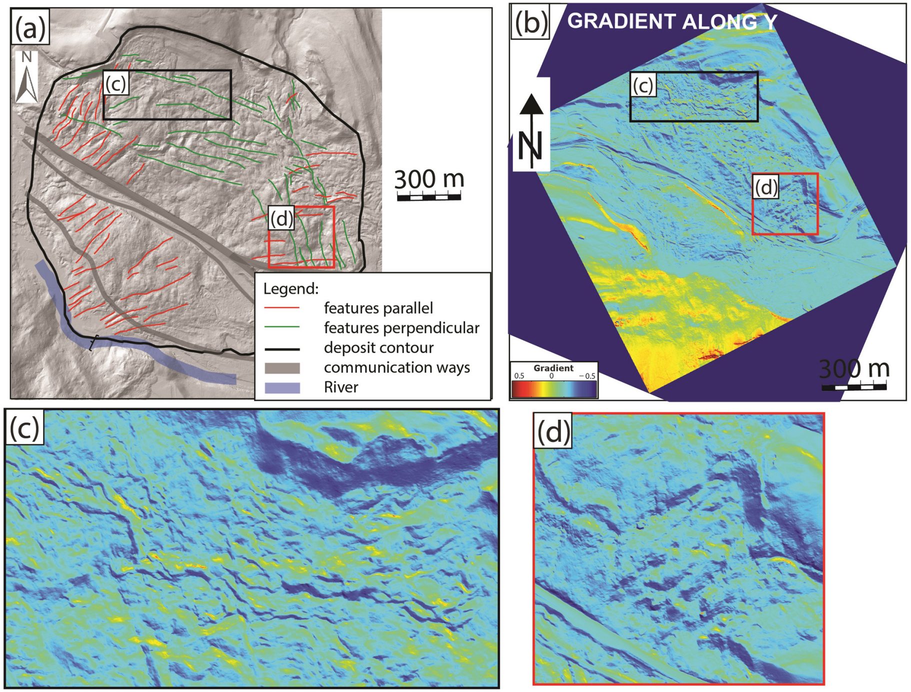

Figure 9. (a) Map of the different features observed on the DEM of Frank Slide deposit; **(b)** Result of the gradient along Y applied to the DEM of Frank Slide; **(c)** zoom on features perpendicular to the flow direction; **(d)** zoom on features parallel to the flow direction.

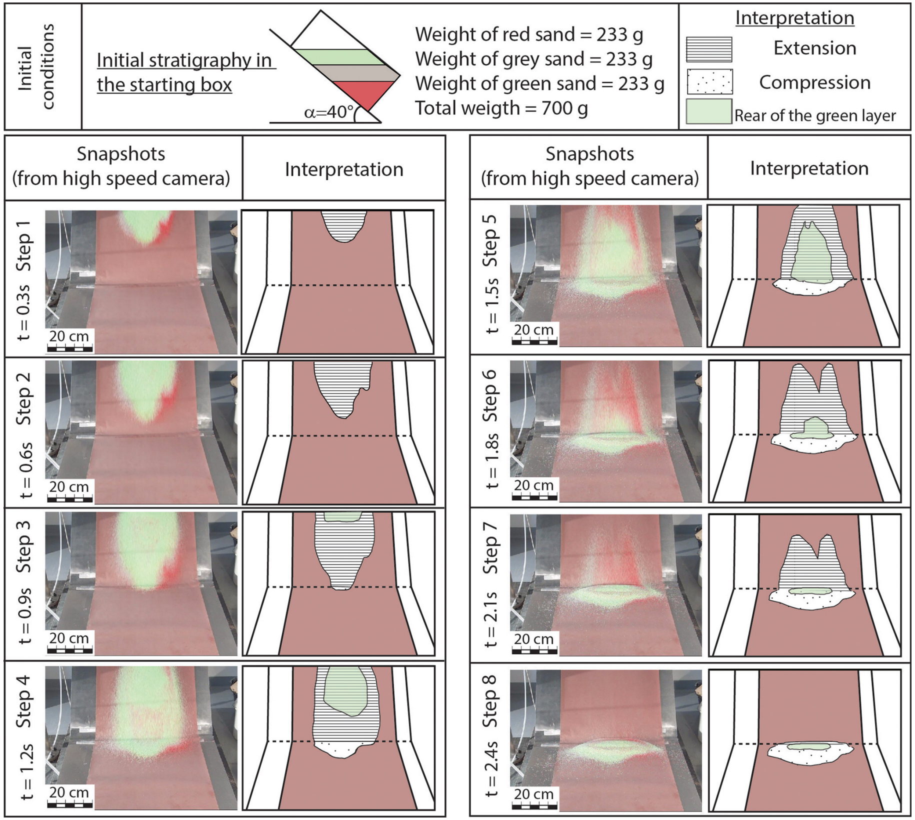

Figure 10. Time laps of an analogue granular flow (0.3 s between each picture). Three colored sand were used during this experiment (red, grey, green). On the left column are the snapshots of the experiment and the right column the interpretation of the flowing mass.

ESURFD

3, 1255–1288, 2015

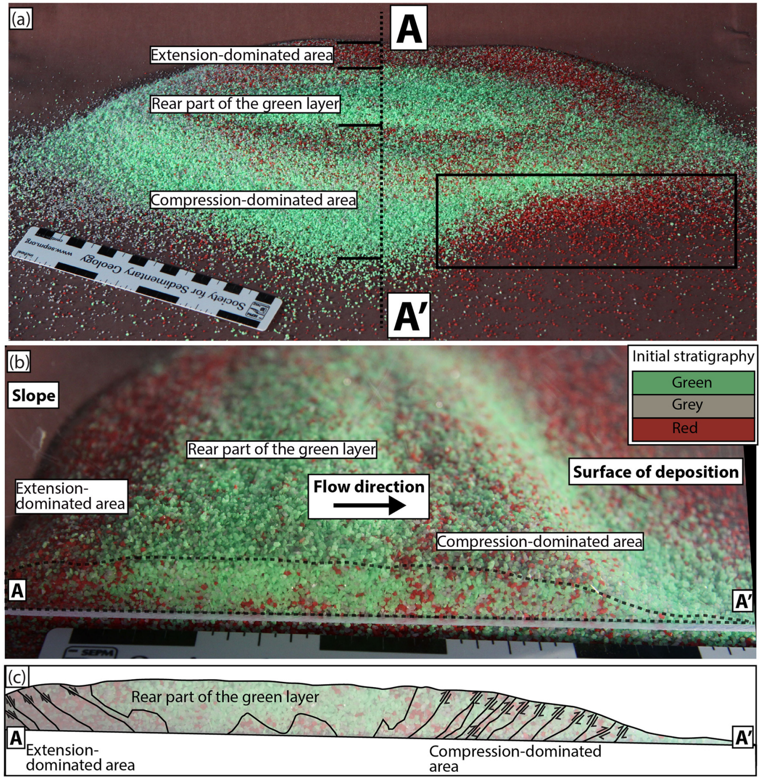

Figure 11. (a) analogue result of the experiment carried with 3 colored sands (Fig. 10); **(b)** cross-section AA′ through the center of the analogue deposit; **(c)** interpretation of the cross-section AA′.

ESURFD
3, 1255–1288, 2015

Analysis of analogue rock avalanche deposits

C. Longchamp et al.

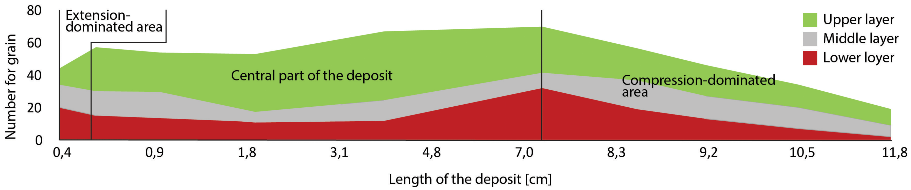

Figure 12. Repartition of the colored sand grains within the deposit.

ESURFD
3, 1255–1288, 2015

Analysis of analogue rock avalanche deposits

C. Longchamp et al.

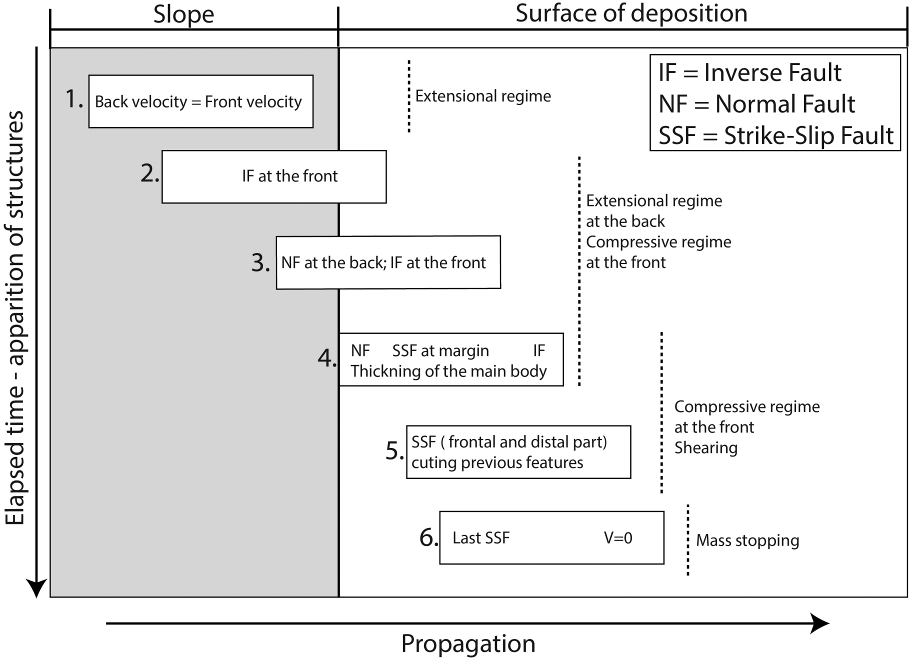

Figure 13. Summarized sketch of the propagation and features appearance of a granular flow in laboratory (modified after Shea and van Wyk de Vries, 2008).

ESURFD
3, 1255–1288, 2015

Analysis of analogue rock avalanche deposits

C. Longchamp et al.